Article

The Effect of Fast Kr Ion Irradiation on the Optical Absorption, Luminescence, and Raman Spectra of BaFBr Crystals

Abdirash Akilbekov [1], Daurzhan Kenbayev [1], Alma Dauletbekova [1], Elena Polisadova [2], Victor Yakovlev [2], Zhakyp Karipbayev [1], Alexey Shalaev [3], Edgars Elsts [4,*] and Anatoli I. Popov [1,4,*]

1   Department of Technical Physics, L.N. Gumilyov Eurasian National University, Satpayev Str. 2, Astana 010008, Kazakhstan; akilbekov_at@enu.kz (A.A.); daurzhankenbayev@gmail.com (D.K.); ak.daukletbekova@gmail.com (A.D.); karipbayev_zht_1@enu.kz (Z.K.)
2   School of Advanced Manufacturing Technologies, National Tomsk Polytechnic University, Tomsk 634050, Russia; polisadova72@gmail.com (E.P.); yak999@rambler.ru (V.Y.)
3   Vinogradov Institute of Geochemistry, Siberian Branch of Russian Academy of Sciences, Favorskii Str. 1a, Irkutsk 664033, Russia; alshal@igc.irk.ru
4   Institute of Solid State Physics, University of Latvia, Kengaraga 8, LV-1063 Riga, Latvia
*   Correspondence: edgars.elsts@cfi.lu.lv (E.E.); popov@latnet.lv (A.I.P.)

Abstract: In this work, using photoluminescence (PL), optical absorption (OA), Raman spectroscopy (RS), and atomic force microscopy (AFM), the radiation damage of BaFBr crystals irradiated with 147 MeV ^{84}Kr ions to fluences (10^{10}–10^{14}) cm^2 was investigated. The manifestations of the oxygen impurity contained in the studied crystals on the effects associated with ion irradiation are also considered. In unirradiated crystals, the PL spectra exhibited bands related to the oxygen impurity. Moreover, it was found that quenching and a shift of the PL maximum occur, which is due to the fact that, with increasing dose, aggregation of defects occurs. Electronic and hole aggregate color centers appear mainly in the bromide sublattice. A detailed study of the Raman spectra and comparison with the corresponding data for KBr single crystals made it possible to reveal the corresponding manifestations of the Raman modes of complex Br_3^--type hole centers.

1. Introduction

So far, the world's best and commercially used storage phosphor for X-ray radiation imaging and dosimetry is barium fluorobromide BaFBr doped with Eu^{2+} as an activator [1–5]. Eu^{2+} doped BaFBr and many related storage phosphors have excellent properties and are most suitable for making various types of imaging plates consisting of phosphor powder dispersed in various organic binders. Image plates were originally developed for X-rays, but are now being extended to other types of ionizing radiation such as neutrons, gamma rays, and electron, proton, and even ion beams [1–10]. It is now clear that such materials have already found many interesting and indeed important applications in many areas of radiation imaging.

When a storage phosphor, for example, based on BaFBr doped with Eu^{2+} impurity, is mixed with a neutron converter, Gd$_2$O$_3$ or ^{6}LiF, it becomes sensitive to thermal neutrons.

Neutron imaging plates (NIP) made of such accumulating phosphors, also including BaFBr$_x$I$_{1−x}$ and Ba$_x$Sr$_{1−x}$FBr, have demonstrated great potential as two-dimensional integrating thermal neutron detectors for neutron radiography and crystallography, etc. [11–14]. It should be noted that, to date, there are only a few studies on the possibility of using BaFBr:Eu^{2+} for ion counting during the microbeam irradiation of heavy ions (protons, carbon, fluorine, and silicon) of biological cells [15]. In particular, it was demonstrated that the energy response of the IP can be used to control ion microbeams with a high dynamic

range. In [16], polycrystalline IP BaFBr:Eu^{2+} films were irradiated with swift heavy ions (^{22}Ne, ^{52}Cr, ^{64}Zn, ^{130}Xe, and ^{238}U) with energies from MeV to GeV. The storage efficiency was studied as a function of ion fluence (10^6–10^{12}) cm^{-2}, and it was found that it decreases with increasing energy loss and is orders of magnitude smaller than for X-rays.

BaFBr has a tetragonal structure perpendicular to the c-axis, of the PbFCl type with the space group P4/nmm [2]. It is generally accepted that electron–hole pairs are generated during irradiation in a storage phosphor. They then recombine either by emitting spontaneous luminescence or by generating a so-called latent image consisting of pairs of electron–hole point defect centers. In BaFX crystals (X = Cl, Br, I), the electrons are either trapped in the bromide vacancy giving $F(Br^-)$ or in the fluoride vacancy giving $F(F^-)$. These centers have C$_{4v}$ and D$_{2d}$ symmetry and their optical characteristics are well established, respectively, but other types of hole defects are practically unexplored, except for those formed at low temperatures, such as self-trapped holes or V$_k$-centers, and a few others [17–26]. It should be noted that the presence of a TSL peak at 363 K complicates the study of color centers (CCs), due to the rapid bleaching [27]. Several types of more complex defects and their various manifestations in luminescent processes have been studied in detail [27,28].

Since BaFBr crystalline materials are used for the production of radiation imaging detectors and have already shown their applicability in the case of ion irradiation, the purpose of this work was to study the effects of ion irradiation on photoluminescence (PL), optical absorption (OA), and Raman spectra (RS) in order to identify which mechanisms of radiation degradation occur. Thus, the aim of our study was to investigate the stable radiation defects in BaFBr crystals stored for a long time in the dark with oxygen impurity, irradiated with 147 MeV ^{84}Kr ions to different fluences at 300 K, using photoluminescence, optical absorption, and Raman spectroscopy.

2. Experiments

BaFBr single crystals were grown using the Shteber method on a special device (Vinogradov Institute of Geochemistry, Siberian Branch of Russian Academy of Sciences SB RAS, Irkutsk, Russia) in a graphite crucible in a helium–fluoride atmosphere using stoichiometric mixtures of BaBr$_2$ and BaF$_2$. However, it is not possible to completely get rid of oxygen, and because of this, in all such prepared crystals several optical absorption bands were detected [29]. The oxygen O^{2-} vacancy defects are known to induce several absorption bands in the ultraviolet up to the exciton fundamental absorption edge. The effect of low concentrations of cationic impurities was further investigated and showed a few additional ways to improve the storage properties of BaFBr [30,31].

Elemental analysis via energy-dispersive X-ray spectroscopy (EDX) was performed using SEM Hitachi TM3030 with Bruker attachment and software quantax 70. EDX analysis found the elements Ba, Br, F, and O (Figure 1). Carbon particles with a peak of 0.3 keV were not considered due to the presence of carbon in the chamber. The grown crystals were colorless and transparent. X-ray diffraction analyses were performed using a D8 ADVANCE ECO X-ray diffractometer having a tube with Cu-anode (Cu Kα, λ = 1.54056 Å, 40 kV, 15 mA) within the 2θ angle range (11.87–83.55°) in 0.01° increments (Figure 2). BrukerAXSDIFFRAC.EVAv.4.2 software and the international database ICDD PDF-2 were used for phase identification and corresponding crystal structure. The obtained results of XRD measurements (Figure 2) are shown in Table 1, thus the formation of BaFBr crystals was confirmed.
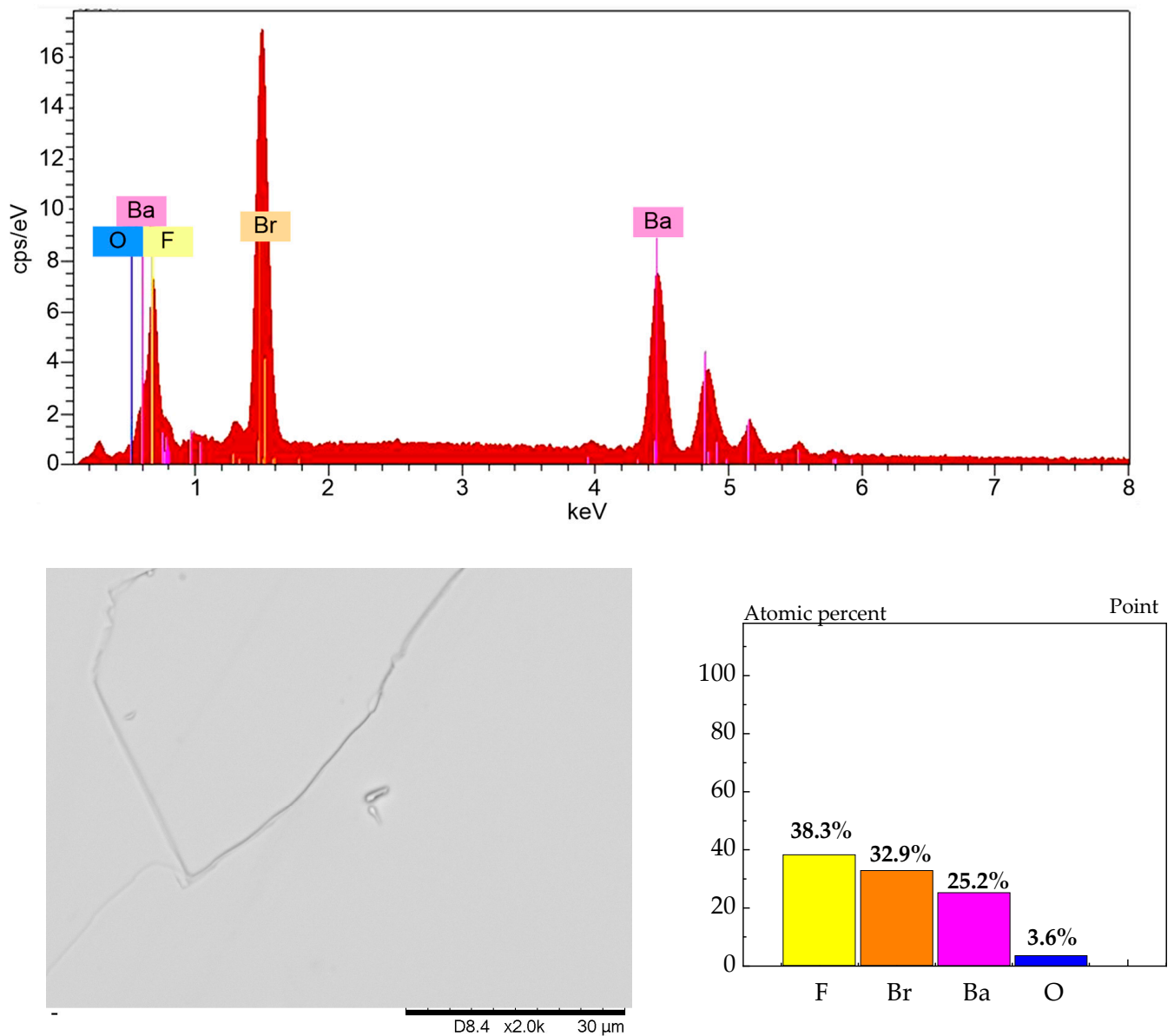
Figure 1. Elemental analysis (EDX) of BaFBr crystals. The lower left corner shows an example of the surface of one of the crystals.

Table 1. Crystallographic parameters of single crystalline BaFBr.

Phase	Structure and Space Group	(hkl)	2θ°	d, Å	Cell Param., Å	Volume, Å³ and Density, g/cm³	Content of Phase %
BaFBr	Tetragonal P4/nmm (129)	102	31.13	2.871	a = 4.5109 b = 4.5109 c = 7.4430 α = β = ϒ = 90°	151.452 and 4.969	100

BaFBr crystal samples were irradiated with 147 MeV ^{84}Kr ions at 300 K to fluences $(10^{10}-10^{14})$ ion/cm^2, at the DC-60 heavy ion accelerator (Nur-Sultan, Kazakhstan). The sample temperature during irradiation was about 70–90 C. Plate samples prepared for irradiation were 10–12 mm long, 9–10 mm wide, and about 1 mm thick. A clear coloration of the samples was observed upon irradiation with sufficiently high ion fluences. At fluences

of 10^{12} ion/cm^2, 10^{13} ion/cm^2, the color was pale pink, while at fluences of 10^{14} ion/cm^2, it was already bright pink.
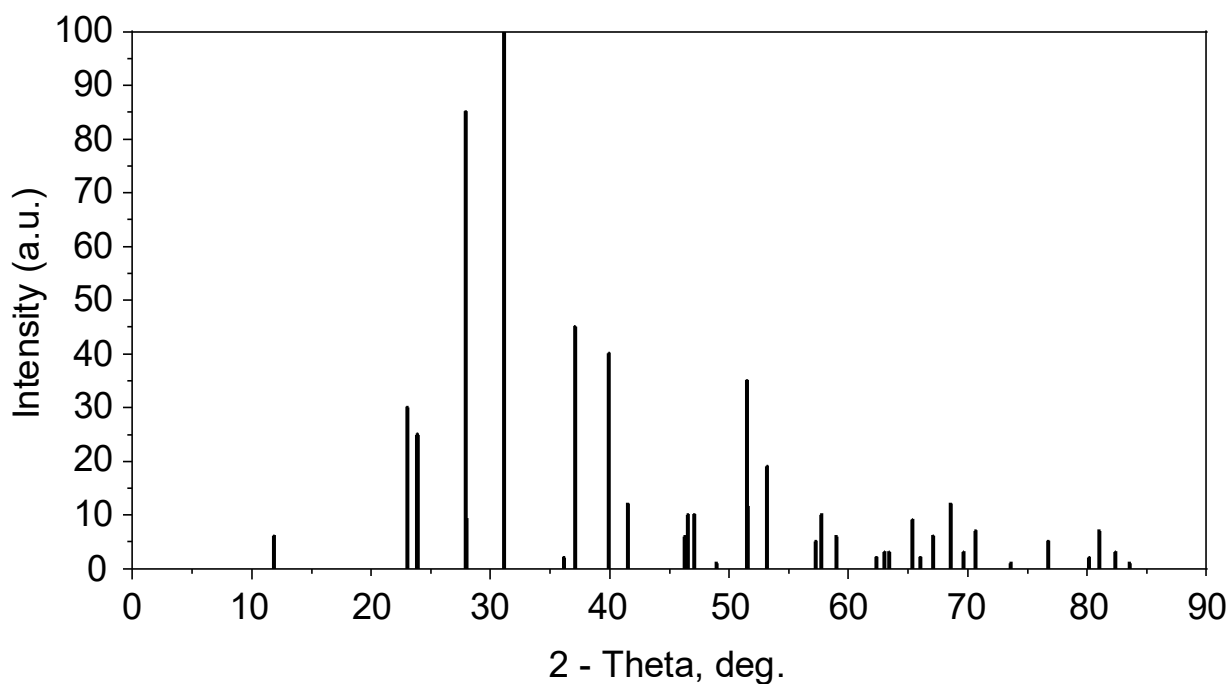

Figure 2. XRD analysis of a BaFBr single crystal sample.

Radiation parameters of ^{84}Kr ions in the BaFBr crystal obtained using code SRIM [32] are presented in Figure 3 and Table 2, where it is clear that electronic energy losses dominate, and most of the ion energy is converted into ionization and electronic excitation energy.
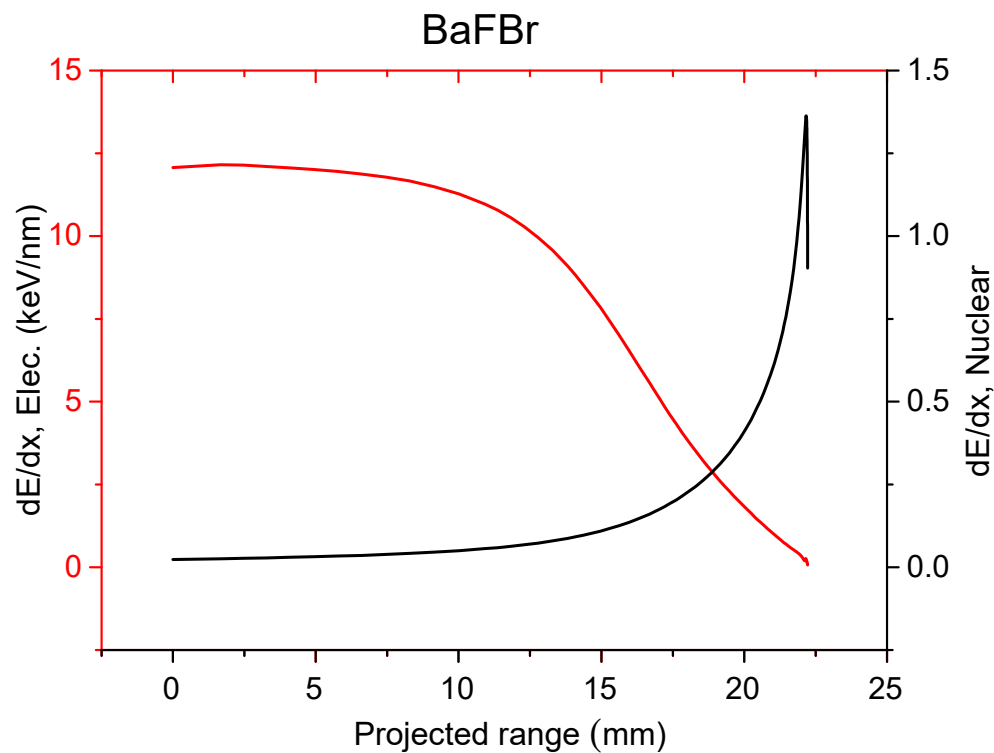

Figure 3. Electronic energy loss (red) and nuclear energy loss (black) of BaFBr crystals irradiated with 147 MeV ^{84}Kr ions.

Table 2. Radiation parameters of 147 MeV ^{84}Kr ions in BaFBr.

Ion	Energy, MeV	$(dE/dx)_e$, keV/nm	$(dE/dx)_n$, keV/nm	R, μm
^{84}Kr	147	12.04	1.36	17.87

The energy losses for ionization and excitation $(dE/dx)_e$ dominate (Table 2) over the energy losses $(dE/dx)_n$ leading to elastic collisions. Note that, in the case of alkali halides such as LiF crystal irradiated in similar conditions with 150 MeV ^{84}Kr ions [33], the Se/Sn ratio = 576, while for BaFBr it is 8.8. As it is well known, for heavy ions with a specific energy above 1 MeV/nucleon, the energy loss is determined via electronic interactions and collisions with the target atoms (nuclear energy loss) are of minor importance [34–37]. As is also well known, heavy ions in solids induce ionization events along the ion path; primary electrons and δ-electrons have a broad spectrum of kinetic energies [38,39]. The maximum electron energy obtained from the krypton ion in BaFBr through analogy with the alkali halide crystals can be estimated using the formula [33,40]:

$$E^e_{max} = \frac{4m_e E_{ion}}{M},$$

(1)

1. Here, m_e is the mass of the electron, M is the mass of the ion, and E_{ion} is the ion energy. For 147 MeV ^{84}Kr ion, $E^e_{max} \approx 3.9$ keV. These electrons form a cascade of secondary δ-electrons. Accordingly [16] the ion energy is thus distributed to a cylindrical region around the ion path typically following a $1/r^2$ law (r denotes the distance from the ion path). Thus, ions eventually generate low-energy electron excitations: electron–hole pairs and excitons. After thermalization of the exciton color centers and other lattice defects are created within a cylindrical region of several tens of nanometers. The possibility of off-center exciton formation in BaFBr and similar materials was theoretically predicted by Baetzold [41]. All this was based on many analogies between excitons in alkali halides and BaFX (X-Br, Cl, and I).

2. The photoluminescence spectra of the crystals were measured according to the standard procedure on an SM2203 spectral fluorimeter (SOLAR, Minsk, Belarus). In this device, the excitation source is a xenon FX-4401 flash lamp (PerkinElmer Optoelectronics GmbH, Wiesbaden, Germany) with a pulse duration of a few microseconds and the light detector is PMT R928 (Hamamatsu, Japan). The control of the device and processing the results of measurements is carried out from the external computer by means of the "Universal" software.

3. The optical absorption spectra were measured using Specord UV-VIS spectrophotometer (SPECORD 250 PLUS) in spectral interval (2.0–6.0) eV. This is double beam spectrophotometer with variable spectral bandwidth and double monochromator, in which the wavelength setting accuracy is ±0.1 nm. An external personal computer using the software WinASPECT is used to control the device and for data processing during measurements.

4. Finally, Raman spectra were measured at room temperature with a Solver Spectrum spectrometer (NT-MDT America Inc, Tempe, AZ 85283, USA), using a solid-state diode laser beam with wavelength of 473 nm (2.62 eV) and a spectral resolution of 1 cm^{-1}. The laser was focused using a 100× objective, forming a spot on the sample surface with a diameter of 2 μm.

3. Results and Discussion

The PL spectra of BaFBr single crystals, previously irradiated with 147 MeV ^{84}Kr ions, were measured under excitation with 280 nm wavelength light and are shown in Figure 4. The spectra were measured after a sufficiently long storage of irradiated crystals at room temperature in the dark.
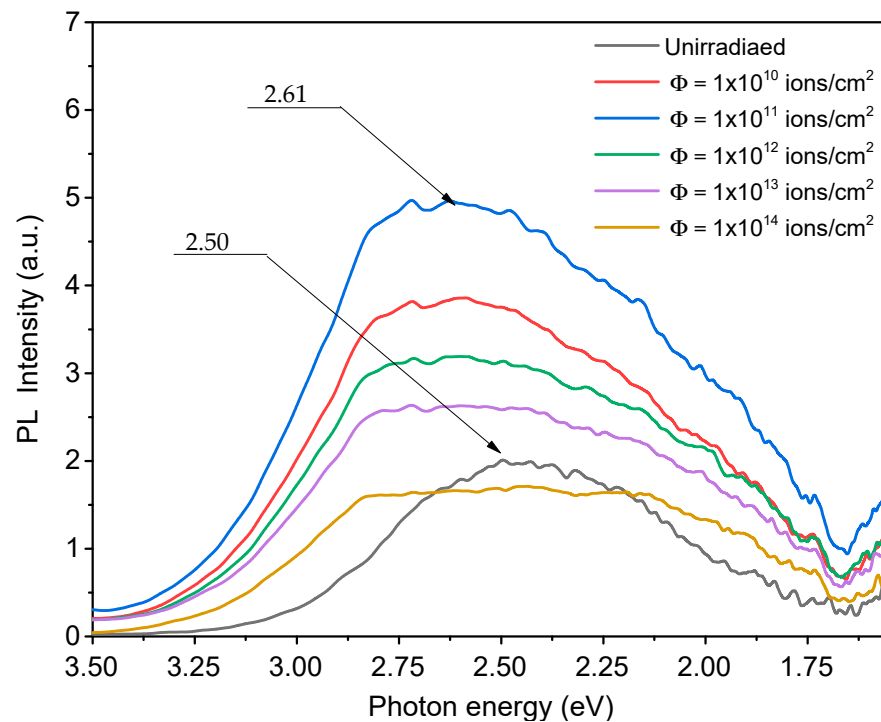
Figure 4. PL spectra of BaFBr crystals irradiated with 147 MeV ^{84}Kr ions at 300 K to fluences 1×10^{10}–1×10^{14} ion/cm^2. Excitation wavelength $\lambda = 280$ nm.

In the PL spectrum, a broad band from 1.5 eV to 3.5 eV is observed, which is also present in the unirradiated crystal, but with a lower intensity. Luminescence intensity increases with the increase in fluence up to a fluence of 10^{11} ion/cm^2. A further increase in fluence leads to a quenching of the PL. A shift of the PL maximum from 2.5 eV (496 nm) to 2.62 eV (473 nm) is also observed. According to [29], PL can be ascribed to oxygen-impurity-bound centers. In work [29], it is shown that the availability of oxygen in the structure of BaFCl and BaFBr crystals leads to the formation of oxygen defect centers. The possibility of two types of oxygen-vacancy center formation has been shown. Type I centers are created when fluorine is replaced by oxygen in neighboring positions with vacancies of CI$^-$ and Br$^-$ ions. Type II centers are formed due to oxygen in the regular sublattice of chlorine or bromine. The summary of the luminescence properties of BaFBr in data analyses in the literature is presented in Table 3.

Then, in unirradiated crystals, the luminescence of the second type of centers with a maximum of 2.5 eV dominates. This means that the oxygen is mostly in the regular bromine site. When the fluence is increased to 10^{11} ion/cm^2, there is an increase in the luminescence intensity of both the first type (2.05 eV) and second type (2.5 eV). However, from a fluence of 10^{12} ion/cm^2, the luminescence suppression begins. At a fluence of 10^{14} ion/cm^2, the shape of the luminescence band develops without pronounced maxima. The decrease in luminescence can be explained via reabsorption in the irradiated layer and via the scattering on macrodefects from irradiated surface layers. Also, the red shift can be explained via the selective reabsorption of luminescence. It should be noted here that the anionic vacancies that are part of oxygen centers can and should capture electrons and transform into *F*-type centers. But, although the irradiation temperature was not so high, this does not allow *F* centers to survive and their most likely fate here is to form dimer centers and metal colloids, as was observed in the case of CaF$_2$ and MgF$_2$ [41–44]. The capturing of electrons by halogen vacancies near oxygen ions also makes it possible to understand the modification of the PL spectrum. According to [45], the development of the peak of thermostimulated luminescence connected with *F*(*F*) centers already begins at 330 K, and the peak itself has a maximum of 360 K.

Table 3. Summary of luminescence properties of BaFBr.

	eV	Comments	Reference
Self-trapped exciton	5.15 4.20		[46]
Oxygen	2.25–2.48	Luminescent center in Br$^-$-rich BaFBr:O^{2-}	[47]
Pb^{2+}	4.77 4.28 2.38	Typical Pb^{2+} emission	[48]
Unknown	1.15 0.91	Excited in the F-absorption band	[49]
Oxygen (?)	3.4	In crystals with a low oxygen concentration	[29]
Eu^{2+}	3.10 3.19	$4f^6 5d^1 \rightarrow 4f^7 (^8S_{7/2})$	[9,50]
O^{2-}-v_a^+ (Type I)	2.5	Excited at 5.0; 6.3; 7.0 eV	[29]
O^{2-}-v_a^+ (Type II)	2.05	Excited at 4.2; 5.28; 6.35 eV	[29]

Table 4 summarizes the available data in the literature on the optical absorption of different point defects in BaFBr. These data are useful and important for understanding and interpreting the experimental data obtained both on irradiated and unirradiated crystals. Figure 5 shows the optical absorption region associated with the absorption of electronic centers. A significant development of absorption in the region 2.2–1.0 eV indicates that the aggregation of simple point defects into complex ones under ion irradiation occurs very efficiently. This is due to the fact that both the heating of the crystals by the beam and the beam flux density effect play a role here. A comparison of the above spectra with the data in the literature allows us to conclude that, in the case of ion irradiation, the same electronic centers are produced as in the case of X-rays or gamma irradiation.
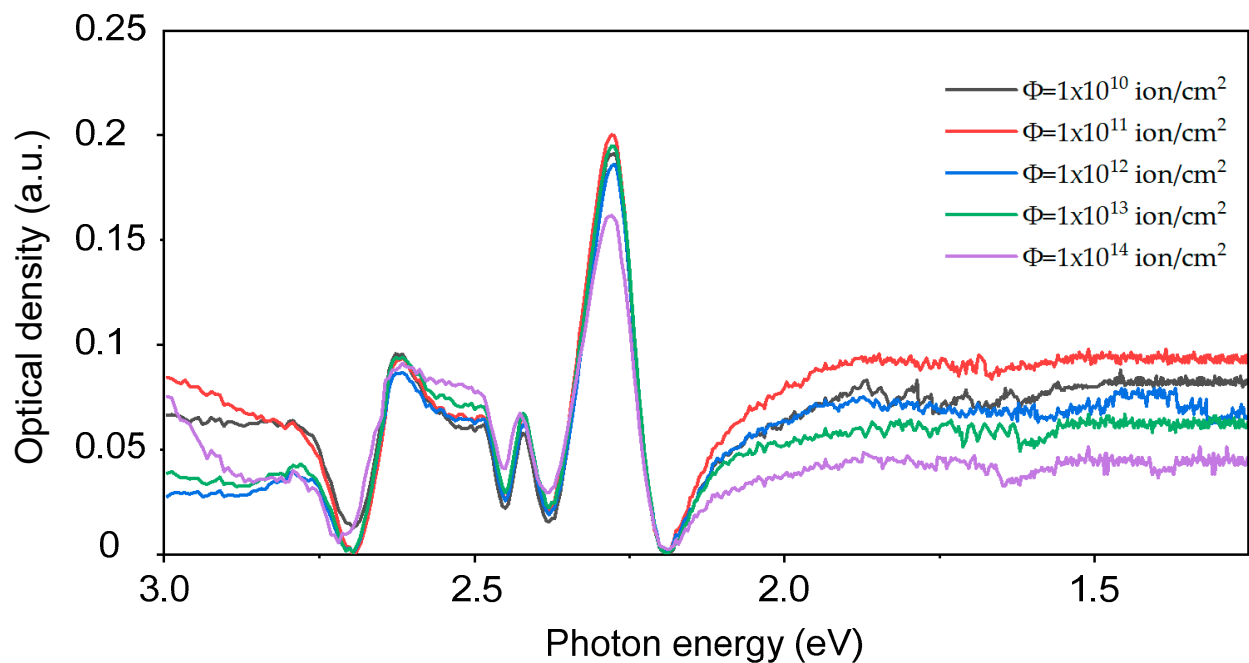

Figure 5. Absorption spectra of BaFBr irradiated with ions 147 MeV ^{84}Kr. Fluence range (1×10^{10} ion/cm^2–1×10^{14}) ion/cm^2.

Table 4. Experimental data on optical absorption bands reported for BaFBr.

	eV	Comments	Reference
Eg	8.20		[51]
exciton	8.15; 7.64		[51]
$O2^- \text{-} v_a^+$ (Type I)	7.0; 6.3; 4.95	2.5 eV emission is excited	[29]
$O2^- \text{-} v_a^+$ (Type II)	6.35; 5.28; 4.2	2.05 eV emission is excited	[29]
V_k center (Br_2^-)	3.4		[3]
?	2.725	After γ-irradiation at RT	[52]
?	2.58	After γ-irradiation at RT	[52]
$F(F^-)$	2.50 2.65 2.72	 X-ray at RT, T_{meas} = 10 K Ad. colored, T_{meas} = 290 K	[53] [49] [28]
$F(Br^-)$	2.15 2.14 2.15 2.18	 γ-ray at RT, T_{meas} = 290 K X-ray at RT, T_{meas} = 10 K X-ray at RT, T_{meas} = 290 K	[53] [52] [49] [28]
R_1	1.89	X-ray at RT, T_{mea} = 290 K	[28]
R_2	1.59	X-ray at RT, T_{mea} = 290 K	[28]
?	1.53	After γ-irradiation at RT	[52]
M	1.36	X-ray at RT, T_{mea} = 290 K	[28]
V_k center (Br_2^-)	1.28		[3]
N_1	1.10	X-ray at RT, T_{mea} = 290 K	[28]
N_2	0.93	X-ray at RT, T_{mea} = 290 K	[28]
Eu^{2+}	4.36; 4.49; 4.67	T_{meas} = 10 K	[49]
?	3.4	X-ray at RT, T_{meas} = 10 K	[49]
?	5.2	X-ray at RT, T_{meas} = 10 K	[49]

It is well known that, in irradiated-by-X-ray crystals of BaFBr, F(Br) centers disappear when stored in the dark at room temperature and the 1.35 eV absorption band associated with the F_2 center increases significantly, and a slight increase in F(F) was also observed [27]. Understanding the thermal instability of F-type centers at room temperature is always important for the correct measurement and processing of images obtained with image plate detectors. The corresponding fading analysis and recipe were proposed and performed more than once for different types of irradiation [54–56]. It is important to note that, in contrast to the conventional irradiation conditions, in the case of ion irradiation at the accelerator, we observed the sharp suppression of defect formation above a fluence of 10^{11}–10^{12} ions/cm^2, which is certainly due to an increase in competing recombination processes and aggregation processes. Therefore, from a 2.2 eV to 1.1 eV spectral range, there is a continuous broad band, which, according to works [27,28], can be assigned to M, R_1, R_2, N_1, and N_2 color centers.

On the other hand, the absorption bands of the aggregate point defects associated with F(F) may also show up here. If, for example, we consider the well-studied LiF, then we can conclude the following, which makes the picture difficult. For example, the absorption band of M (F_2) centers (457.8 nm, 2.71 eV) in LiF crystals coincides with the absorption of F_3^+ centers. It should be highlighted that the M band includes the absorption contributions of F_2 and F_3^+ defects. For the most colored LiF crystals, the contributions of $F_3(R_1)$ at around 316 nm (3.92 eV), $F_3(R_2)$ at around 374 nm 3.32 eV, and the $F_4(N)$ band contributions at 517 nm 2.39 eV and 547 nm 2.27 eV are also relevant [57–60].

In parallel to the electron point defects of *F*-type, complementary hole defects are also produced. In our case, these are aggregate hole centers. The spectral range 3.5–6.5 eV (Figure 6) was chosen purposefully. It is in this region of the spectrum that the so-called *V*-type absorption bands of KBr crystals are found [61]. The similar absorption of fluorine aggregates in alkali and alkaline earth fluorides is known to be situated in the VUV region of the spectrum [62–65]; therefore, in this work, only the Raman spectra of bromine aggregates are discussed.
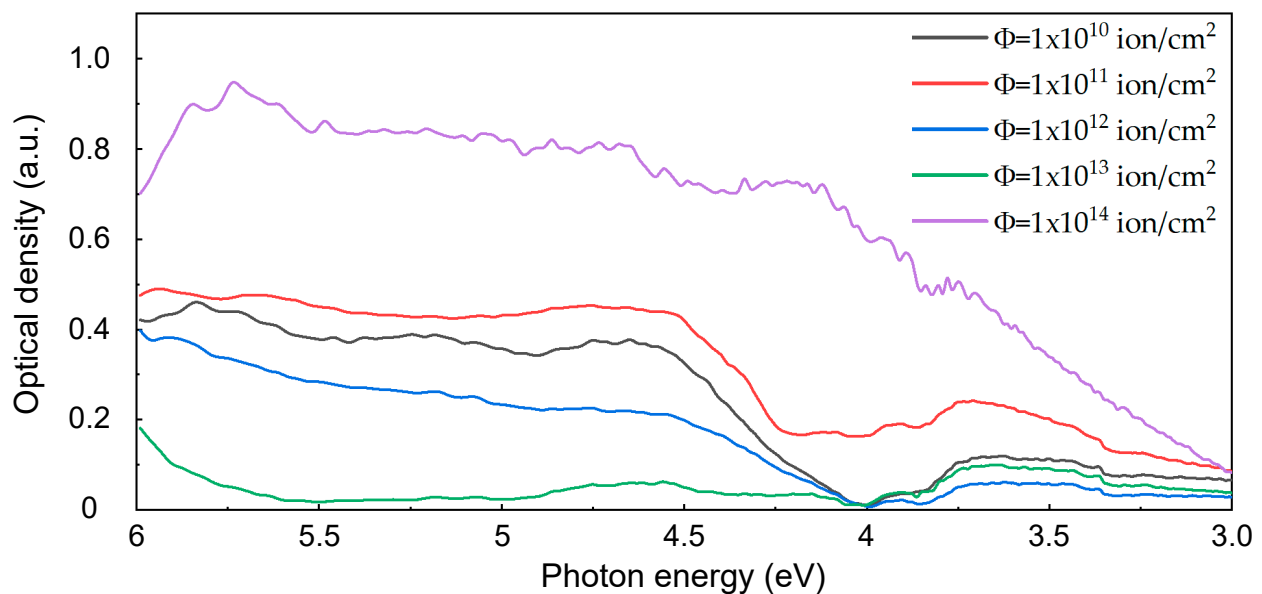
Figure 6. Absorption spectra of BaFBr irradiated with 147 MeV ^{84}Kr ions. Fluence range $(1 \times 10^{10} – 1 \times 10^{14})$ ion/cm^2.

In the Raman spectra of X-irradiated KBr crystals, the part induced by V-centers was determined. It consists of bands at 175 cm^{-1}, 265 cm^{-1}, and 349 cm^{-1} (the first overtone of the 175 cm^{-1} mode) [66]. Thus, for bromide compounds, Raman modes were observed with frequencies of about 175 cm^{-1} for Br$_3^-$ (valence vibration) and 265 cm^{-1} for Br$_2$ type centers that encompass any poly-halide ion such as Br$_5$ or even higher poly-ions. In the Raman spectra of BaFBr irradiated with 147 MeV ^{84}Kr ions, we see all these vibrational modes; Figure 7a–c.

Compared with the results on the study of aggregate hole centers in KBr, we can assume that the absorption band with a maximum of 4.5 eV is associated with Br$_3^-$ centers and 5.5 eV with di-H centers [61].

In the following work, we will show how luminescent impurities, namely Eu^{2+}, affect the efficiency of defect formation, which determines the detection efficiency. In the case of scintillation crystals CsI-Tl, it is known that low concentrations of the Tl$^+$ impurity increase the efficiency of the formation of stable defects under swift heavy ion irradiation, while high concentrations completely suppress it [67]. The relevant principles of luminescent protection against defect creation due to the recombination of hot or relaxed electrons and holes were clearly formulated in [68]. We note that, in order to study primary pairs of Frenkel defects in BaFX crystals (X = Cl, Br, I) and their corresponding thermal stability, it is necessary to carry out the necessary irradiations at liquid helium temperatures. Such methods are well developed for alkali metal halides [69–73], but have not yet been applied to BaFX compounds, so such experiments have already begun.
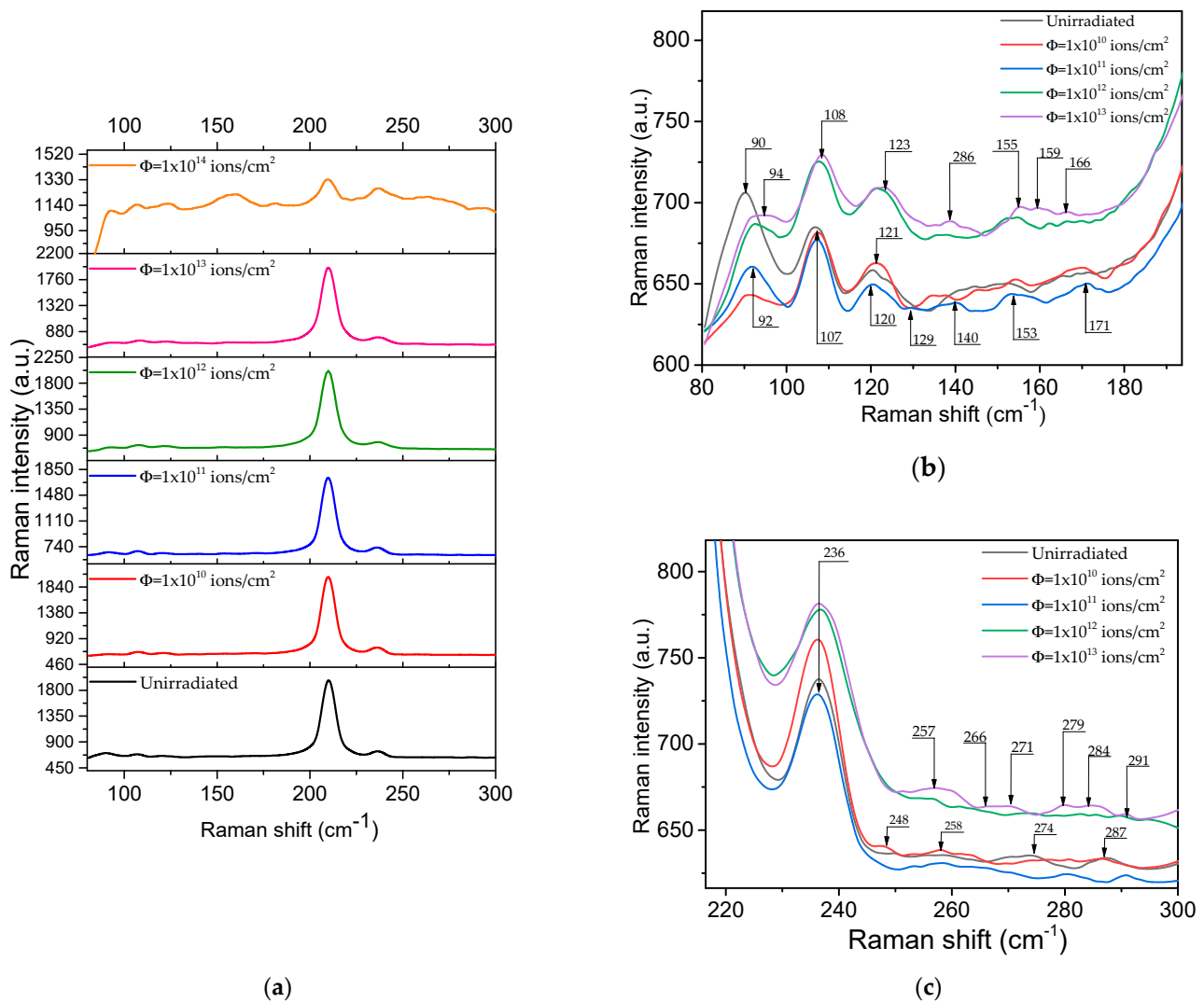
Figure 7. Raman spectra of BaFBr as a function of ion fluence, shown for different spectral ranges: 80–300 cm^{-1} (**a**), 80–195 cm^{-1} (**b**) and 210–300 cm^{-1} (**c**).

4. Conclusions

For the studied BaFBr crystals, both unirradiated and irradiated with Kr ions with an energy of 147 MeV and stored for a long time in the dark, the presence of an oxygen impurity was found. A broad complex emission band from 1.5 to 3.5 eV was observed in the PL spectrum, which is also found in an unirradiated crystal, but with a lower intensity. This PL band includes the luminescence of two oxygen-related centers with different structures. Then, in unirradiated crystals, the luminescence of centers of the second type dominates with a maximum of 2.5 eV. This means that the oxygen is located mainly in the usual bromine site. As the fluence increases to 10^{11} ions/cm^2, an increase in the luminescence intensity of oxygen-vacancy defects of both the first (2.05 eV) and second (2.5 eV) types is observed. At a fluence of 10^{12} ion/cm^2, luminescence suppression begins. At a fluence of 10^{14} ion/cm^2, the shape of the luminescence band develops without pronounced maxima, which indicates a significant modification of the luminescence centers. The irradiation with SHI leads to the sharp suppression of defect formation above a fluence of 10^{11}–10^{12} ions/cm^2. This is due to an increase in competing recombination processes and aggregation processes. The analysis of the absorption and Raman spectra of the samples irradiated with Kr swift ions showed the creation of electronic and hole aggregate of point defects. Compared with the results of the previous study of aggregate hole point defects in

KBr, we can assume that the absorption band with a maximum of 4.5 eV is associated with Br_3^- enters and 5.5 eV with di-H centers.

References

1. Nicklaus, E.; Fischer, F. *F*-Centres of Two Types in BaFCl Crystals. *Phys. Status Solidi B* **1972**, *52*, 453–460. [CrossRef]
2. Beck, H.P. A study on mixed halide compounds MFX (M = Ca, Sr, Eu, Ba; X = Cl, Br, I). *J. Solid State Chem.* **1976**, *17*, 275–282. [CrossRef]
3. Koschnick, F.K.; Spaeth, J.-M.; Eachus, R.S. The influence of oxide impurity on the generation by X-irradiation of F centres in BaFBr. *J. Phys. Condens. Matter* **1992**, *11*, 3015–3029. [CrossRef]
4. Takebe, M.; Abe, K. A novel particle identification with an imaging plate. *Nucl. Instrum. Methods Phys. Res. Sect. A* **1994**, *345*, 606–608. [CrossRef]
5. Takebe, M.; Abe, K. A particle energy determination with an imaging plate. *Nucl. Instrum. Methods Phys. Res. Sect. A* **1995**, *359*, 625–627. [CrossRef]
6. Takebe, M.; Abe, K.; Kondo, Y.; Satoh, Y.; Souda, M. Identification of Ionizing Radiation with an Imaging Plate Using Two-Wavelength Stimulation Light. *JJAP* **1995**, *34*, 4197–4199. [CrossRef]
7. Taniguchi, S.; Yamadera, A.; Nakamura, T.; Fukumura, A. Measurement of radiation tracks for particle and energy identification by using imaging plate. *Nucl. Instrum. Methods Phys. Res. Sect. A* **1998**, *413*, 119–126. [CrossRef]
8. Kobayashi, H.; Shibata, H.; Eguchi, H.; Satoh, M.; Etoh, M.; Takebe, M.; Abe, K. Deterioration of photo-stimulated luminescence signals from materials by radiation. *Nucl. Instrum. Methods Phys. Res. Sect. B* **2000**, *164–165*, 938–943. [CrossRef]
9. Popov, A.I.; Zimmermann, J.; McIntyre, G.J.; Wilkinson, C. Photostimulated luminescence properties of neutron image plates. *Opt. Mater.* **2016**, *59*, 83–86. [CrossRef]
10. Golovin, D.O.; Mirfayzi, S.R.; Shokita, S.; Abe, Y.; Lan, Z.; Arikawa, Y.; Morace, A.; Pikuz, T.A.; Yogo, A. Calibration of imaging plates sensitivity to high energy photons and ions for laser-plasma interaction sources. *JINST* **2021**, *16*, T02005. [CrossRef]
11. Wilkinson, C.; Gabriel, A.; Lehmann, M.S.; Zemb, T.; Ne, F. Image plate neutron detector. In Proceedings of the SPIE 1737, Neutrons, X-rays, and Gamma Rays: Imaging Detectors, Material Characterization Techniques, and Applications, San Diego, CA, USA, 2 February 1993. [CrossRef]
12. Niimura, N.; Karasawa, Y.; Tanaka, I.; Miyahara, J.; Takahashi, K.; Saito, H.; Koizumi, S.; Hidaka, M. An imaging plate neutron detector. *Nucl. Instrum. Methods Phys. Res. Sect. A* **1994**, *349*, 521–525. [CrossRef]
13. Cipriani, F.; Castagna, J.-C.; Claustre, L.; Wilkinson, C.; Lehmann, M.S. Large area neutron and X-ray image-plate detectors for macromolecular biology. *Nucl. Instrum. Methods Phys. Res. Sect. A* **1997**, *392*, 471–474. [CrossRef]
14. Wilkinson, C.; Cowan, J.A.; Myles, D.A.A.; Cipriani, F.; McIntyre, G.J. VIVALDI—A thermal-neutron laue diffractometer for physics, chemistry and materials science. *Neutron News* **2002**, *13*, 37–41. [CrossRef]
15. Tosaki, M.; Nakamura, M.; Hirose, M.; Matsumoto, H. Application of heavy-ion microbeam system at Kyoto University: Energy response for imaging plate by single ion irradiation. *Nucl. Instrum. Methods Phys. Res. Sect. B* **2011**, *269*, 3145–3148. [CrossRef]
16. Batentschuk, M.; Winnacker, A.; Schwartz, K.; Trautmann, C. Storage efficiency of BaFBr:Eu^{2+} image plates irradiated by swift heavy ions. *J. Lumin.* **2007**, *125*, 40–44. [CrossRef]
17. Zimmermann, J.; Kolb, R.; Hesse, S.; Schlapp, M.; Schmechel, R.; von Seggern, H. Preparation-induced *F*-centre transformation in BaFBr: Eu^{2+}. *J. Phys. D Appl. Phys.* **2004**, *37*, 2352. [CrossRef]
18. Koschnick, F.K.; Spaeth, J.M.; Eachus, R.S.; McDugle, W.G.; Nuttall RH, D. Experimental evidence for the aggregation of photostimulable centers in BaFBr:Eu^{2+} single crystals by cross relaxation spectroscopy. *Phys. Rev. Lett.* **1991**, *67*, 3571. [CrossRef]

19. Takahashi, K. Progress in science and technology on photostimulable BaFX: Eu^{2+} (X = Cl, Br, I) and imaging plates. *J. Lumin.* **2002**, *100*, 307–315. [CrossRef]
20. Spaeth, J.M. Recent developments in X-ray storage phosphor materials. *Radiat. Meas.* **2001**, *33*, 527–532. [CrossRef]
21. Spaeth, J.M.; Hangleiter, T.; Koschnick, F.K.; Pawlik, T. X-ray storage phosphors. *Radiat. Eff. Defects Solids* **1995**, *135*, 1–10. [CrossRef]
22. Hall, C.; Kamenskikh, I.A.; Gurvich, A.M.; Munro, I.H.; Mikhailin, V.V.; Worgan, J.S. Phosphors for luminescent image plates. *J. X-ray Sci. Technol.* **1996**, *6*, 48–62. [CrossRef]
23. Nanto, H.; Okada, G. Optically stimulated luminescence dosimeters: Principles, phosphors and applications. *Jpn. J. Appl. Phys.* **2022**, *62*, 010505. [CrossRef]
24. Popov, A.I.; Kotomin, E.A.; Maier, J. Analysis of self-trapped hole mobility in alkali halides and metal halides. *Solid State Ion.* **2017**, *302*, 3–6. [CrossRef]
25. Sidorenko, A.V.; Bos, A.J.J.; Dorenbos, P.; Van Eijk, C.W.E.; Rodnyi, P.A.; Berezovskaya, I.V.; Popov, A.I. Storage properties of Ce^{3+} doped haloborate phosphors enriched with ^{10}B isotope. *J. Appl. Phys.* **2004**, *95*, 7898–7902. [CrossRef]
26. Harrison, A.; Lane, L.C.; Templer, R.H.; Seddon, J.M. Mechanism of charge storage and luminescence stimulation in BaFBr: RE phosphors. *Nucl. Instrum. Methods Phys. Res. Sect. A Accel. Spectrom. Detect. Assoc. Equip.* **1991**, *310*, 220–223. [CrossRef]
27. Zhao, W.; Mi, Y.M.; Song, Z.F.; Su, M.Z. Color Centers in the Near Infrared Region in Crystals MFX (M = Ba, Sr; X = Cl, Br). *J. Solid State Chem.* **1993**, *103*, 415–419. [CrossRef]
28. Kurobori, T.K.T.; Kawabe, M.K.M.; Liu, M.L.M.; Hirose, Y.H.Y. Experimental evidence for the aggregation of the near-IR bands in BaFBr: Eu^{2+} single crystals. *JJAP* **2000**, *39*, L629–L632. [CrossRef]
29. Radzhabov, E.; Otroshok, V. Optical spectra of oxygen defects in BaFCl and BaFBr crystals. *J. Phys. Chem. Solids* **1995**, *56*, 1–7. [CrossRef]
30. Shalaev, A.A.; Radzhabov, E.A. Single crystal growth of BaFBr:Eu storage phosphor with alkali impurities. *J. Cryst. Growth* **2005**, *275*, e775–e777. [CrossRef]
31. Shalaev, A.; Radzhabov, E.A.; Shabanova, E. Introducing alkali impurities into BaFBr:Eu^{2+} crystals and their effect on photo-stimulated luminescence. *Nucl. Instrum. Methods Phys. Res. Sect. A Accel. Spectrom. Detect. Assoc. Equip.* **2002**, *486*, 471–473. [CrossRef]
32. Ziegler, J.F.; Ziegler, M.D.; Biersak, J.P. SRIM–The stopping and range of ions in matter. *Nucl. Instrum. Methods Phys. Res. Sect. B* **2010**, *268*, 1818–1823. [CrossRef]
33. Schwartz, K.; Sorokin, M.V.; Dauletbekova, A.; Baizhumanov, M.; Akilbekov, A.; Zdorovets, M. Energy loss effect on color center creation in LiF crystals under irradiation with ^{12}C, ^{14}N, ^{40}Ar, ^{84}Kr, and ^{130}Xe ions. *Nucl. Instrum. Methods Phys. Res. Sect. B* **2015**, *359*, 53–56. [CrossRef]
34. Itoh, H.; Duffy, D.M.; Khakshouri, S.; Stoneham, A.M. Making tracks: Electronic excitation roles in forming swift heavy ion tracks. *J. Phys. Condens. Matter* **2009**, *21*, 474205. [CrossRef] [PubMed]
35. Schwartz, K.; Trautmann, C.; Steckenreiter, T.; Geiß, O.; Krämer, M. Damage and track morphology in LiF crystals irradiated with GeV ions. *Phys. Rev. B* **1998**, *58*, 11232. [CrossRef]
36. Szenes, G.; Pászti, F.; Péter, Á.; Popov, A.I. Tracks induced in TeO$_2$ by heavy ions at low velocities. *Nucl. Instrum. Methods Phys. Res. Sect. B Beam Interact. Mater. At.* **2000**, *166*, 949–953. [CrossRef]
37. Kimura, K.; Sharma, S.; Popov, A. Fast electron–hole plasma luminescence from track-cores in heavy-ion irradiated wide-band-gap crystals. *Nucl. Instrum. Methods Phys. Res. Sect. B Beam Interact. Mater. At.* **2002**, *191*, 48–53. [CrossRef]
38. Medvedev, N.A.; Volkov, A.E.; Schwartz, K.; Trautmann, C. Effect of spatial redistribution of valence holes on the formation of a defect halo of swift heavy-ion tracks in LiF. *Phys. Rev. B* **2013**, *87*, 104103. [CrossRef]
39. Kimura, K.; Sharma, S.; Popov, A.I. Novel ultra-fast luminescence from incipient ion tracks of insulator crystals: Electron–hole plasma formation in the track core. *Radiat. Meas.* **2001**, *34*, 99–103. [CrossRef]
40. Lushchik, C.; Lushchik, A. Evolution of Anion and Cation Excitons in Alkali Halide Crystals. *Phys. Solid State* **2018**, *60*, 1487–1505. [CrossRef]
41. Kotomin, E.A.; Kuzovkov, V.N.; Popov, A.I. The kinetics of defect aggregation and metal colloid formation in ionic solids under irradiation. *Radiat. Eff. Defects Solids* **2001**, *155*, 113–125. [CrossRef]
42. Huisinga, M.; Bouchaala, N.; Bennewitz, R.; Kotomin, E.A.; Reichling, M.; Kuzovkov, V.N.; Von Niessen, W. The kinetics of CaF$_2$ metallization induced by low-energy electron irradiation. *Nucl. Instrum. Methods Phys. Res. Sect. B Beam Interact. Mater. At.* **1998**, *141*, 79–84. [CrossRef]
43. Hazem, R.; Izerrouken, M. Proton irradiation-induced defect aggregation and metallic nanoparticles in CaF$_2$ single-crystal. *Radiat. Phys. Chem.* **2023**, *204*, 110643. [CrossRef]
44. Batool, A.; Izerrouken, M.; Aisida, S.O.; Hussain, J.; Ahmad, I.; Afzal, M.Q.; Zhao, T.K. Effect of Ca colloids on in-situ ionoluminescence of CaF$_2$ single crystals. *Nucl. Instrum. Methods Phys. Res. Sect. B Beam Interact. Mater. At.* **2020**, *476*, 40–43. [CrossRef]
45. Ye, B.; Lin, J.H.; Su, M.Z. Two types of F-centers in BaFBr. *J. Lumin.* **1988**, *40–41*, 323–324. [CrossRef]
46. Radzhabov, E.A. Decay of exciton emission in BaFBr crystals. *J. Phys. Condens. Matter* **1995**, *7*, 1597–1602. [CrossRef]
47. Dong, Y.; Ren, M.; Mu, C.; Lin, J.H.; Su, M.Z. Luminescent center in Br$^-$-rich BaFBr:O^{2-}. *J. Lumin.* **1999**, *81*, 231–235. [CrossRef]

48. Van Dijken, A.; Folkerts, H.F.; Blasse, G. Evidence for D-band emission from Pb^{2+} in alkaline-earth fluorohalides with the PbFCl structure. *J. Lumin.* **1997**, *72–74*, 660–661. [CrossRef]

49. Hangleiter, T.; Koschnick, F.K.; Spaeth, J.-M.; Nuttall, R.H.D.; Eachus, R.S. Temperature dependence of the photostimulated luminescence of X-irradiate BaFBr: Eu^{2+}. *J. Phys. Condens. Matter* **1990**, *2*, 6837–6846. [CrossRef]

50. Brixner, L.H.; Bierlein, J.D.; Johnson, V. Eu^{2+} fluorescence and its application in medical X-ray intensifying screens. Chapter 2. *Curr. Top. Mater. Sci.* **1980**, *4*, 47–87.

51. Nicklaus, E. Optical properties of some alkaline earth halides. *Phys. Stat. Sol. A* **1979**, *53*, 217–224. [CrossRef]

52. Reddy, M.; Somaiah, K.; Babu, H.V. Thermoluminescence of BaFBr crystals. *Phys. Stat. Sol. A* **1979**, *54*, 245–250. [CrossRef]

53. Iwabuchi, Y.; Umemoto, C.; Takahashi, K.; Shionoya, S. Photostimulated luminescence process in BaFBr:Eu^{2+} containing $F(Br^{-})$ and $F(F^{-})$ centers. *J. Lumin.* **1991**, *48–49*, 481–484. [CrossRef]

54. Ohuchi, H.; Yamadera, A. Development of a functional equation to correct fading in imaging plates. *Radiat. Meas.* **2002**, *35*, 135–142. [CrossRef]

55. Ohuchi, H.; Yamadera, A. Dependence of fading patterns of photo-stimulated luminescence from imaging plates on radiation, energy, and image reader. *Nucl. Instrum. Methods Phys. Res. Sect. A Accel. Spectrom. Detect. Assoc. Equip.* **2002**, *490*, 573–582. [CrossRef]

56. Maddox, B.R.; Park, H.S.; Remington, B.A.; Izumi, N.; Chen, S.; Chen, C.; Ma, Q. High-energy x-ray backlighter spectrum measurements using calibrated image plates. *Rev. Sci. Instrum.* **2011**, *82*, 023111. [CrossRef] [PubMed]

57. Vincenti, M.A.; Baldacchini, G.; Kalinov, V.S.; Montereali, R.M.; Voitovich, A.P. Spectroscopic investigation of F, F_2 and F_3^{+} color centers in gamma irradiated lithium fluoride crystals. In *IOP Conference Series: Materials Science and Engineering*; IOP Publishing: Bristol, UK, 2010; Volume 15, p. 012053. [CrossRef]

58. Lisitsyna, L.A.; Lisitsyn, V.M.; Korepanov, V.I.; Grechkina, T.V. The efficiency of formation of primary radiation defects in LiF and MgF_2 crystals. *Opt. Spectrosc.* **2004**, *96*, 230–234. [CrossRef]

59. Nahum, J.; Wiegand, D.A. Optical properties of some F-aggregate centers in LiF. *Phys. Rev.* **1967**, *154*, 817. [CrossRef]

60. Sankowska, M.; Bilski, P.; Marczewska, B.; Zhydachevskyy, Y. Influence of Elevated Temperature on Color Centers in LiF Crystals and Their Photoluminescence. *Materials* **2023**, *16*, 1489. [CrossRef]

61. Akilbekov, A.; Elango, A. Low-Temperature Pair Associates of *H* Centres in KBr. *Phys. Stat. Sol. B* **1984**, *122*, 715–723. [CrossRef]

62. Radzhabov, E.A. F_3^{-} molecular ions in fluoride crystals. *Opt. Spectrosc.* **2016**, *120*, 294–299. [CrossRef]

63. Assylbayev, R.; Lushchik, A.; Lushchik, C.; Kudryavtseva, I.; Shablonin, E.; Vasil'chenko, E.; Zdorovets, M. Structural defects caused by swift ions in fluorite single crystals. *Opt. Mater.* **2018**, *75*, 196–203. [CrossRef]

64. Vasil'chenko, E.; Kudryavtseva, I.; Lushchik, A.; Lushchik, C.; Nagirnyi, V. Selective creation of colour centres and peaks of thermally stimulated luminescence by VUV photons in LiF single crystals. *Phys. Status Solidi (C)* **2005**, *2*, 405–408. [CrossRef]

65. Lushchik, A.; Kudryavtseva, I.; Liblik, P.; Lushchik, C.; Nepomnyashchikh, A.I.; Schwartz, K.; Vasil'chenko, E. Electronic and ionic processes in LiF: Mg, Ti and LiF single crystals. *Radiat. Meas.* **2008**, *43*, 157–161. [CrossRef]

66. Rzepka, E.; Doualan, J.L.; Lefrant, S.; Taurel, L. Raman scattering induced by V centres in KBr. *J. Phys. C Solid State Phys.* **1982**, *15*, L119–L123. [CrossRef]

67. Popov, A.I.; Balanzat, E. F centre production in CsI and CsI–Tl crystals under Kr ion irradiation at 15 K. *Nucl. Instrum. Methods Phys. Res. Sect. B Beam Interact. Mater. At.* **2000**, *166*, 545–549. [CrossRef]

68. Lushchik, A.; Feldbach, E.; Galajev, S.; Kärner, T.; Liblik, P.; Lushchik, C.; Vasil'chenko, E. Some aspects of radiation resistance of wide-gap metal oxides. *Radiat. Meas.* **2007**, *42*, 792–797. [CrossRef]

69. Lushchik, C.; Kolk, J.; Lushchik, A.; Lushchik, N.; Tajirov, M.; Vasil'chenko, E. Decay of excitons into long-lived F, H and α, I pairs in KCl. *Phys. Stat. Solidi (B)* **1982**, *114*, 103–111. [CrossRef]

70. Lushchik, A.; Lushchik, C.; Vasil'chenko, E.; Popov, A.I. Radiation creation of cation defects in alkali halide crystals: Review and today's concept. *Low Temp. Phys.* **2018**, *44*, 269–277. [CrossRef]

71. Kirm, M.; Lushchik, A.; Lushchik, C.; Martinson, I.; Nagirnyi, V.; Vasil'chenko, E. Creation of groups of spatially correlated defects in a KBr crystal at 8 K. *J. Phys. Condens. Matter* **1998**, *10*, 3509. [CrossRef]

72. Kotomin, E.A.; Popov, A.I.; Eglitis, R.I. Correlated annealing of radiation defects in alkali halide crystals. *J. Phys. Condens. Matter* **1992**, *4*, 5901. [CrossRef]

73. Kuzovkov, V.N.; Popov, A.I.; Kotomin, E.A.; Moskina, A.M.; Vasilchenko, E.; Lushchik, A. Theoretical analysis of the kinetics of low-temperature defect recombination in alkali halide crystals. *Low Temp. Phys.* **2016**, *42*, 588–593. [CrossRef]